Eur. Phys. J. D **1**, 129-137 (1998)

THE EUROPEAN PHYSICAL JOURNAL D

Rare-gas-induced broadening and shift of two-photon transitions to intermediate (n = 9−14) Rydberg states of atomic thallium*

G. Hermann[a], B. Kaulakys[b], and G. Mahr

I. Physikalisches Institut der Justus-Liebig-Universität Giessen, Heinrich-Buff-Ring 16, 35392 Giessen, Germany

Received: 6 August 1997 / Revised in final form: 29 November 1997 / Accepted: 11 December 1997

Abstract. Results of broadening and shift measurements of Doppler-free two-photon lines for transitions from the ground state to the $n\mathrm{P}_J$ Rydberg states with intermediate principle quantum numbers of atomic thallium perturbed by rare gases are reported. The rates show a distinct behaviour in this range of principle quantum numbers and significant dependence on the total angular momentum of the upper nP state. The experimental results are compared with calculations using a Van der Waals potential and a superposition of polarization and Fermi potentials. Additionally, broadening and shift rates of the transition Tl $6\mathrm{P}_{3/2}$–$9\mathrm{P}_{3/2}$ have been measured for quadrupolar as well as for mainly scalar excitation. The rates for both kinds of excitation coincide within the limits of error reflecting the small perturbation of the $6\mathrm{P}_{3/2}$ state compared to that of the upper $9\mathrm{P}_{3/2}$ state.

PACS. 32.70.-n Intensities and shapes of atomic spectral lines – 31.50.+w Excited states – 34.20.-b Interatomic and intermolecular potentials and forces, potential energy surfaces for collisions

1 Introduction

The studies of broadening and shift of spectral lines associated with transitions between the ground state and highly excited states of atoms in gases have been performed continually for relatively long time. Reviews of works in this field can be found in the papers [1–3]. Measurements of the broadening and shift rates provide information about the interaction potentials between the radiating (or absorbing) and perturbing atoms [4–6]. Broadening and shift of the Rydberg levels by neutral perturbing atomic particles have a number of distinctive features, associated with the fact that interaction between the Rydberg atom and the particle consists of two quasi-independent interactions: interaction of the perturbing particle with the core of the Rydberg atom and with the Rydberg electron. The theory of pressure shift of the Rydberg levels originates with Fermi [7], has been continued by Firsov [8] and extended by Alekseev and Sobelman [9] to include broadening. Later the theory of collisional broadening and shift of transitions to Rydberg states has been developed by Omont [10] for high Rydberg states. It has been improved and extended in paper [11] to states with intermediate and low principle quantum numbers and more recently generalized [12,13] taking into account the finite size of the interaction potential between the valence electron and the perturber and the anisotropy of the Rydberg-perturber interaction potential. These theories relate the spectral line shapes with the parameters of the interaction potentials and show that in the case of transitions between the ground state and high Rydberg states the spectral line shapes are entirely determined by the perturbation of the Rydberg states. Broadening and shift of the high Rydberg states are independent on the quantum numbers and are determined only by the type of perturbing atom. Measurements of such transitions are in reasonable agreement with the theoretical results [1–3].

However, measurements of the recent years of the collisional broadening of transitions to states with intermediate principle quantum numbers show a significant dependence on the orbital [14,15] and total [16] angular momentum of the upper state. This indicates the influence of the anisotropy of the Rydberg-perturber potential on the collisional process of Rydberg atoms with neutral perturbers and on the broadening and shift of the Rydberg states even after the angular average over the atomic collisions. Moreover, for transitions from the ground to low states collisional perturbation of the ground state may have essential influence. In such a case the dependence of line broadening and shift on the rank of the transition operator, mentioned for the first time in a theoretical work of Cooper [17] and analyzed in detail using the density matrix formalism by Omont [18,19], may appear.

* This paper is dedicated to Prof. Dr. D.Sc. Dr. h.c. mult. A. Scharmann on the occasion of his 70th birthday

[a] e-mail: Gerd.Hermann@exp1.physik.uni-giessen.de

[b] Alexander von Humboldt Fellow. Permanent address: Institute of Theoretical Physics and Astronomy, A. Goštauto 12, 2600 Vilnius, Lithuania

It was the aim of this work to investigate experimentally the dependencies of broadening and shift of spectral lines corresponding to transitions in the transient range to the Rydberg states with the above mentioned asymptotic behaviour on the quantum numbers of the involved states, on the anisotropy of the interaction potential, and on the type of excitation, *i.e.* on the rank of the transition operator.

Here a completed study of the impact broadening and shift of thallium transitions involving intermediate ^2P_J fine structure states applying Doppler-free two-photon spectroscopy is reported. In addition, the transitions $6P_{1/2}$–$nP_{1/2,3/2}$ ($n = 9-14$) and $6P_{3/2}$–$9P_{3/2}$ perturbed by rare gases of low density were investigated with high precision.

For Tl one- and two-photon transitions into low lying states with small principle quantum numbers $n \leq 9$ broadening and shift rates caused by various rare gases have already been published [16,20–24]. A few data exist for transitions into states with $n = 10$, too [16,25]. With the experiments of this work the data are improved and extended to the especially interesting states with intermediate principle quantum numbers. Some of these results are reported in a short form in paper [26].

In this study the experimental results are related with calculations and discussed in detail. By comparing the experimental results with calculations for various interatomic potentials the reliability of these theoretical potentials can be checked. The precise measurement under identical experimental conditions and over a wide range of principle quantum numbers of transitions into $P_{1/2}$ and $P_{3/2}$ states of the same doublet with almost equal radial wave functions allows the thorough analysis of the effects on pressure broadening resulting from the anisotropy of the interaction potential. It is an advantage of the measurements on Tl that due to the large fine structure splitting inelastic collisions, usually complicating the theoretical analysis and discussion, can be neglected even for intermediate states. Furthermore, the dependence of line broadening and shift on the rank of the transition operator is investigated on the $6P_{3/2}$–$9P_{3/2}$ line. Quadrupolar as well as mainly scalar excitation can be obtained for this transition using appropriate polarizations of the exciting laser beams in the two-photon experiment [27].

2 Experimental set-up

The experimental arrangement is shown in Figure 1. An electrically heated quartz-cell contained the thallium vapour. The Tl vapour pressure could be adjusted with the temperature of an independently heated reservoir. For the chosen temperature of about 970 K the vapour pressure is 10.9 Pa corresponding to Tl number densities of 8.1×10^{14} cm^{-3} in the $6P_{1/2}$ and 7.8×10^{9} cm^{-3} in the $6P_{3/2}$ state. The cell was connected to a vacuum and gas filling system *via* a heated valve sealed by polished quartz surfaces. The gas pressure has been measured with a temperature stabilized capacitance manometer (MKS Baratron) with an accuracy better than 0.5%.

The beam of a stabilized cw-dye-ring laser (Spectra Physics 380D) with a line-width of less than 1 MHz operated with Stilben 3 ($6P_{1/2}$–$nP_{1/2,3/2}$; $n = 9-12$), Stilben 1 ($6P_{1/2}$–$nP_{1/2,3/2}$; $n = 12-14$), and Rhodamine 110 ($6P_{3/2}$–$9P_{3/2}$) was focused into this quartz cell. After crossing the cell the laser beam was reflected and refocused by a spherical mirror. For the measurements on the $6P_{3/2}$–$9P_{3/2}$ transition one or two additional quarter-wave plates were included in the paths of the exciting laser beams to get the desired circular polarizations. Circular polarizations rotating in the same direction result in pure quadrupolar two-photon excitation, whereas for opposite directions of the circular polarization the ratio of scalar to quadrupolar transitions is optimized for maximum scalar excitation. Additional polarizers were needed for decoupling the laser system.

The Doppler-free two-photon absorption signal was detected by measuring the fluorescence on the $\lambda = 378$ nm ($7S_{1/2}$–$6P_{1/2}$) and $\lambda = 352$ nm ($6D_J$–$6P_{3/2}$) lines. Stray light of the laser and infrared radiation of the oven could be sufficiently reduced by a Schott UG1 filter and an ethylene glycol filled quartz cuvette, respectively. The signal-to-noise ratio was improved by using lock-in technique in combination with intensity modulation of the retroreflected laser beam.

For stable wavelength calibration of the spectra a marker cavity (confocal interferometer, free spectral range 150.4 MHz) actively locked to an I_2-stabilized He-Ne laser was used. Long-term drifts of the calibration marks smaller than 1 MHz made possible the accurate determination of line broadening and, in particular, of line shift. In order to reduce the errors resulting from a small nonlinearity of the laser scan additional calibration marks were recorded during the measurements on the $6P_{3/2}$–$9P_{3/2}$ transition. For that purpose, sidebands in the laser frequency spectrum with separations of 20 MHz were generated by means of an electro-optical phase modulator. Three sidebands on each side of the carrier could be reliably detected with the marker cavity for a modulation index of about three (Fig. 2).

The fluorescence signal as well as the transmission of the marker cavity were digitized with a data acquisition board (Datalog DAP 1200) and stored into a personal computer used both as a 16-bit multi-channel analyzer and as laser scan-control unit.

3 Measurements and results

The broadening and shift rates for the two-photon transitions Tl $6P_{1/2}$–$nP_{1/2,3/2}$ ($n = 9-14$) perturbed by rare gases (He, Ne, Ar, Kr, Xe) are presented in Table 1. Due to the nuclear spin $I = 1/2$ of ^{205}Tl several hyperfine (HFS) lines exist. In the case of the $6P_{1/2}$–$nP_{1/2}$ transitions the strongest of the two HFS-lines ($F = 1 \rightarrow F' = 1$) was scanned, whereas for the $6P_{1/2}$–$nP_{3/2}$ transitions we used the most separated line ($F = 0 \rightarrow F' = 2$) of the HFS spectrum. The scan range was 760 MHz, the scanning time 75 s and the cell temperature 1040 K. For each

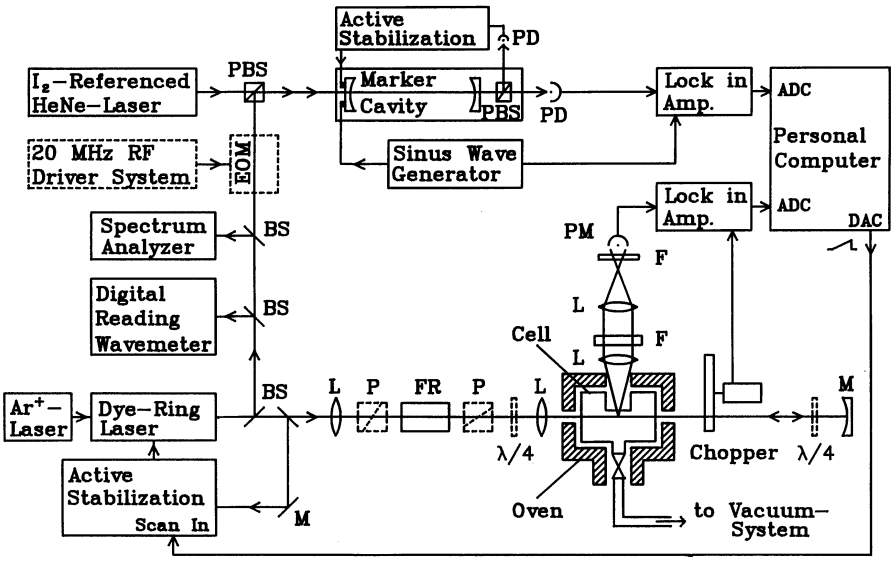

Fig. 1. Experimental set-up. BS, beam splitter; EOM, electro-optical phase modulator; F, optical filter; FR, Faraday rotator; L, lens; M, mirror; PBS, polarizing beam splitter or beam combiner; P, polarizer; PD, photodiode; PM, photomultiplier; $\lambda/4$, quarter-wave plate; ADC, DAC, analog-to-digital and digital-to-analog converter. Components marked with dashed lines were only used for measurements on the $6P_{3/2}$–$9P_{3/2}$ transition.

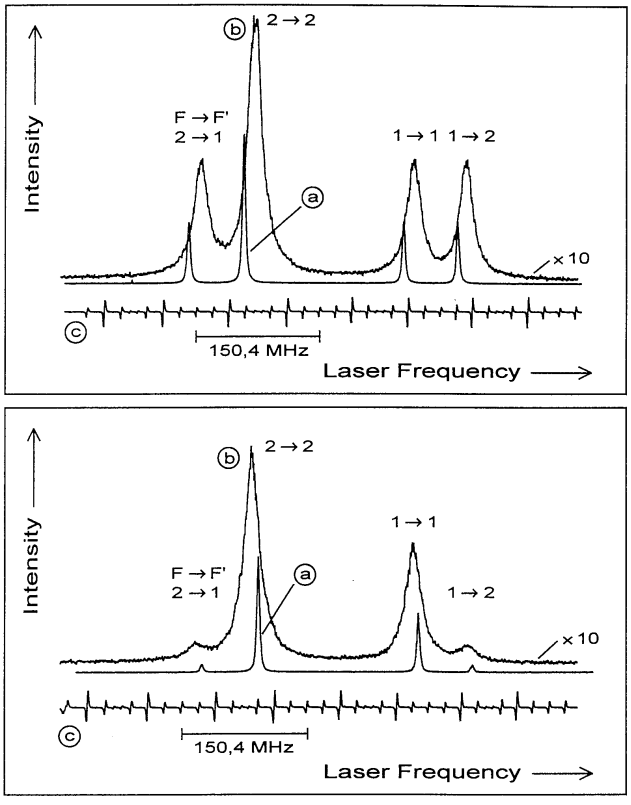

Fig. 2. Two-photon absorption signals of the transition Tl $6P_{3/2}$–$9P_{3/2}$ perturbed by Helium for excitation with two counter-propagating laser beams with same circular polarization (upper drawing) and of the transition Tl $6P_{3/2}$–$9P_{3/2}$ perturbed by Argon for opposite polarization of the laser beams (lower drawing): (a) without admixture of rare gas, (b) perturbed by 0.8 Torr Helium and 0.8 Torr Argon, respectively, (c) wavelength calibration marks

transition measurements were performed at four or five different rare gas pressures up to 10 Torr.

Additionally, measurements on the Tl $6P_{3/2}$–$9P_{3/2}$ two-photon transition were performed for studying the dependence of line broadening and shift on the rank of the transition operator. The HFS excitation spectra of this transition consist of four components (see Fig. 2). For the chosen circular polarizations of the exciting laser beams the contributions of scalar and quadrupolar transitions to the excitation of the HFS-components are listed in Table 2. All components were scanned together because of their small spectral separations. The scan range was 620 MHz, the scanning time 150 s. In this case measurements were performed with a cell temperature of 1036 K for Helium and Argon perturbers at gas pressures between 0 and 1 Torr in 0.1 Torr steps. The maximum pressure of 1 Torr was chosen in order to avoid too wide overlapping of the HFS-components.

The Lorentzian halfwidth γ_{TP} and the shift $\Delta/2$ of the two-photon lines were obtained from least-square fits. Thereby, in the case of the $6P_{3/2}$–$9P_{3/2}$ transition the sum of four Lorentzian profiles was fitted to the experimental data. The halfwidth γ_{TP} contains several contributions and is given by

$$\gamma_{\mathrm{TP}} = (\gamma_f + \gamma_{\mathrm{Tl}} + \gamma)/2\,. \qquad (1)$$

The natural linewidth γ_f and the Tl self-broadening γ_{Tl} for a given Tl vapour pressure are constants, whereas γ varies with the rare gas pressure. The same statements are true for the line shift as well.

The halfwidth γ_{TP} and the shift $\Delta/2$ showed the expected linear dependence on the rare gas number density N. The broadening rates γ/N and shift rates Δ/N resulting from the linear regressions are presented in Table 1 and Table 3 . The errors given in these tables contain the double standard deviation of the linear regression. The total estimated errors of most results are in the range

Table 1. Comparison of experimental broadening and shift rates of two-photon transitions Tl $6P_{1/2}$–$nP_{1/2,\ 3/2}$ ($n = 9 - 14$) perturbed by rare gases (Exp) with calculated rates for Van der Waals potential (C_6) and a superposition of polarisation and Fermi potentials (PF).

		Broadening rate $(\gamma/N)/10^{-20}$ cm^2					Shift rate $(\Delta/N)/10^{-20}$ cm^2				
Transition		Helium	Neon	Argon	Krypton	Xenon	Helium	Neon	Argon	Krypton	Xenon
$6P_{1/2}$–$9P_{1/2}$	C_6	—	—	10.03	9.95	11.07	—	—	−3.64	−3.61	−4.02
	PF	20.42	4.46	15.28	11.47	9.89	7.76	2.39	0.00	0.00	0.00
	Exp	13.97(42)	3.75(20)	17.44(48)	16.24(58)	16.55(71)	12.41(31)	2.65(18)	−6.35(31)	−4.07(32)	−3.80(40)
$6P_{1/2}$–$9P_{3/2}$	C_6	—	—	10.35	10.26	11.42	—	—	−3.76	−3.73	−4.15
	PF	19.9	4.5	15.07	12.37	10.67	6.55	2.10	0.00	0.00	0.00
	Exp	14.87(53)	4.95(23)	17.54(50)	15.63(64)	15.79(56)	10.00(29)	1.99(16)	−5.84(29)	−3.95(25)	−3.94(28)
$6P_{1/2}$–$10P_{1/2}$	C_6	—	—	13.72	13.61	15.14	—	—	−4.98	−4.94	−5.50
	PF	13.7	4.08	27.25	24.73	21.32	16.85	2.28	0.00	0.00	0.00
	Exp	10.28(42)	3.03(9)	24.14(71)	31.2(12)	28.24(82)	15.58(39)	2.63(13)	−12.52(48)	−5.20(32)	−5.75(38)
$6P_{1/2}$–$10P_{3/2}$	C_6	—	—	14.08	13.97	15.54	—	—	−5.12	−5.07	−5.65
	PF	15.3	4.20	23.5	25.83	22.72	15.15	2.16	0.00	0.00	0.00
	Exp	11.17(49)	3.72(16)	25.20(93)	26.64(92)	25.87(83)	13.57(32)	2.28(13)	−11.42(31)	−5.15(32)	−5.48(33)
$6P_{1/2}$–$11P_{1/2}$	C_6	—	—	17.81	17.66	19.66	—	—	−6.47	−6.42	−7.14
	PF	9.5	3.83	26.6	46.14	40.56	20.14	2.04	−15.01	0.00	0.00
	Exp	6.86(26)	2.86(13)	23.79(90)	54.9(16)	44.8(11)	17.05(32)	2.39(13)	−18.96(48)	−15.00(80)	−5.60(41)
$6P_{1/2}$–$11P_{3/2}$	C_6	—	—	18.22	18.07	20.11	—	—	−6.62	−6.56	−7.30
	PF	10.5	3.90	27.9	40.96	42.53	19.35	1.98	−12.73	0.00	0.00
	Exp	8.36(32)	3.35(18)	26.58(86)	48.2(13)	39.6(13)	15.32(37)	2.06(14)	−18.07(50)	−9.90(58)	−6.92(34)
$6P_{1/2}$–$12P_{1/2}$	C_6	—	—	22.29	22.11	24.60	—	—	−8.10	−8.03	−8.94
	PF	6.88	3.68	21.4	63.22	70.44	21.13	1.84	−26.52	0.00	0.00
	Exp	5.49(19)	2.87(13)	21.65(73)	63.7(20)	88.9(25)	17.94(35)	2.25(9)	−23.77(50)	−30.34(89)	−11.6(10)
$6P_{1/2}$–$12P_{3/2}$	C_6	—	—	22.71	22.52	25.06	—	—	−8.25	−8.18	−9.11
	PF	7.67	3.73	24.2	54.3	66.17	20.80	1.81	−23.48	0.00	0.00
	Exp	6.99(32)	3.18(16)	24.2(11)	66.4(21)	66.3(21)	16.26(36)	1.99(7)	−23.29(66)	−22.76(97)	−8.24(68)
$6P_{1/2}$–$13P_{1/2}$	C_6	—	—	27.10	26.88	29.91	—	—	−9.84	−9.76	−10.86
	PF	5.41	3.59	18.3	61.16	104.74	21.43	1.70	−32.31	−28.42	0.00
	Exp	4.71(18)	2.89(12)	18.89(80)	59.5(22)	129.5(46)	18.27(30)	2.10(10)	−26.83(56)	−43.5(19)	−35.1(26)
$6P_{1/2}$–$13P_{3/2}$	C_6	—	—	27.56	27.34	30.42	—	—	−10.01	−9.93	−11.05
	PF	5.93	3.63	19.6	60.0	88.0	21.28	1.68	−30.48	−23.99	0.00
	Exp	6.28(31)	3.19(19)	20.71(85)	71.8(34)	109.7(46)	16.86(34)	1.93(12)	−26.78(60)	−38.2(19)	−17.9(27)
$6P_{1/2}$–$14P_{1/2}$	C_6	—	—	32.26	32.00	35.61	—	—	−11.72	−11.63	−12.94
	PF	4.55	3.54	15.32	50.2	119.61	21.51	1.59	−35.01	−49.46	0.00
	Exp	4.28(26)	—	15.72(85)	50.4(30)	142.1(65)	18.75(44)	—	−28.55(64)	−52.1(30)	−64.5(51)
$6P_{1/2}$–$14P_{3/2}$	C_6	—	—	32.78	32.52	36.18	—	—	−11.91	−11.81	−13.14
	PF	4.90	3.56	16.7	55.1	105.5	21.44	1.58	−34.06	−41.80	0.00
	Exp	5.94(47)	—	17.96(85)	66.1(36)	153.4(85)	17.47(42)	—	−29.03(63)	−50.7(32)	−41.7(46)

Table 2. Relative intensities of the HFS lines in the $6P_{3/2}$–$9P_{3/2}$ spectra and relative contributions of scalar and quadrupolar transitions to the total line intensities

Circular polarization of two exciting laser beams with	HFS transition F → F'	Relative intensity	Relative contributions to the total intensity by scalar transitions	quadrupolar transitions
Same orientation	1 → 1	3	0	100
	1 → 2	3	0	100
	2 → 1	3	0	100
	2 → 2	7	0	100
Opposite orientation	1 → 1	27	88.9	11.1
	1 → 2	3	0	100
	2 → 1	3	0	100
	2 → 2	47	85.1	14.9

Table 3. Observed broadening rates γ/N and shift rates Δ/N for two HFS lines $F \to F'$ of the $6P_{3/2}$–$9P_{3/2}$ transition perturbed by He (upper part of table) and Ar (lower part of table), respectively.

	$(\gamma/N)/10^{-20}$ cm^2		$(\Delta/N)/10^{-20}$ cm^2	
Excitation	$F = 2 \to F' = 2$	$F = 1 \to F' = 1$	$F = 2 \to F' = 2$	$F = 1 \to F' = 1$
mainly scalar	15.21(41)	15.08(39)	10.45(49)	10.46(54)
quadrupolar	15.25(39)	15.03(39)	10.32(60)	10.40(62)
mainly scalar	17.16(55)	17.57(54)	−5.97(46)	−6.08(40)
quadrupolar	17.35(41)	17.19(49)	−5.94(46)	−5.73(46)

1.5–3% resulting from the precision of the temperature and pressure measurement (1%) and from other error sources like time-of-flight broadening, the residual Zeeman splitting due to stray magnetic fields.

As the rare gas number density N was calculated by means of the cell temperature measured with a

Table 4. Dipole polarizability α [31] and scattering length L [32] of the rare gases used for calculations (a_0 is Bohr radius).

	Helium	Neon	Argon	Krypton	Xenon
α/a_0^3	1.384	2.663	11.08	16.73	27,29
L/a_0	1.17	0.204	−1.55	−3.50	−6.50

thermocouple on the surface of the quartz cell a possible difference between the surface temperature and the temperature in the excitation region results in an additional error. The estimated uncertainty of the temperature in the excitation region of ±20 K is, however, of no importance for the comparisons of the measured rates within this paper, *e.g.* between transitions into $P_{1/2}$ and $P_{3/2}$ states, because the cell temperature was controlled within ±5 K. If these rates are compared with the results of other authors, the additional errors of 2% should be taken into account. For $n = 9$ and 10 these results differ from those of reference [16] because of systematic errors of the previous values resulting from the measurements of the cell and reservoir temperatures, furthermore, partly from the signal distortion in the electronic readout system.

4 Discussion

For the given experimental parameters (low rare gas pressures and observation of the line center) the experimental results can be discussed within the framework of the impact theory. The line shape is given by a Lorentzian profile with halfwidth γ and shift Δ,

$$\gamma = 2N \langle v\, \sigma_\mathrm{b}(v) \rangle \tag{2}$$

$$\Delta = N \langle v\, \sigma_\mathrm{s}(v) \rangle \tag{3}$$

where N is the perturbing particle density and the brackets denote the average over the Maxwellian distribution of relative velocities v of the interacting atoms. The broadening and shift of an optical line corresponding to a transition from the ground state is mainly determined by the perturbation of the upper state. The broadening and shift cross sections σ_b and σ_s are given for a degenerated upper level with angular momentum J_f by [19]

$$\sigma_\mathrm{b} - I\sigma_\mathrm{s} = 2\pi \int_0^\infty \Pi(b,v) b\, \mathrm{d}b \tag{4}$$

$$\Pi(b,v) = 1 - (2J_\mathrm{f}+1)^{-1} \sum_{m_\mathrm{f}} \langle m_\mathrm{f}|S(b,v)|m_\mathrm{f}\rangle \tag{5}$$

where b is the impact parameter, m_f is the magnetic quantum number, and S is the collision S matrix connecting the wave functions Ψ before and $\Psi' = S\Psi$ after the collision.

4.1 Isotropic interaction potentials

For an isotropic interaction potential $V(R)$, as given in the case of the $6P_{1/2}$–$nP_{1/2}$ transitions, the S matrix elements in equation (5) can be expressed by the phase shift η_f in the form $\langle m_\mathrm{f}|S|m_\mathrm{f}\rangle = \mathrm{e}^{-I\eta_\mathrm{f}}$ and equations (4) and (5) result in the well known expressions of the adiabatic phase shift theory

$$\sigma_\mathrm{b}(v) = 2\pi \int_0^\infty [1 - \cos\eta_\mathrm{f}(v,b)]\, b\, \mathrm{d}b \tag{6}$$

$$\sigma_\mathrm{s}(v) = -2\pi \int_0^\infty \sin\eta_\mathrm{f}(v,b)\; b\, \mathrm{d}b \tag{7}$$

$$\eta(b) = -\frac{2}{v} \int_b^\infty \frac{V(R)/\hbar}{\sqrt{1 - b^2/R^2}}\, \mathrm{d}R\,. \tag{8}$$

Broadening rates γ/N and shift rates Δ/N were calculated from these expressions assuming as interaction potentials a Van der Waals potential $V(R) = C_6 R^{-6}$ as well as a superposition of a polarization potential and a Fermi pseudopotential.

The final formulas used for the Van der Waals potential are [28,29]

$$\gamma/N = 7.90\,(2\pi c)^{-1} \bar{v}^{3/5} |C_6/\hbar|^{2/5} \tag{9}$$

$$\Delta/N = -2.87\,(2\pi c)^{-1} \bar{v}^{3/5} |C_6/\hbar|^{2/5} \tag{10}$$

where $\bar{v} = (8kT/\pi\mu)^{1/2}$ is the mean relative velocity (with k being the Boltzmann constant and μ the reduced mass of the radiator-perturber system). For the Van der Waals coefficient C_6 the approximation $C_6 = -\alpha e^2 \langle r^2 \rangle$ was used with α being the dipole polarizability of the perturber listed in Table 4, e the elementary charge and $\langle r^2 \rangle$ the expectation value of r^2 for the thallium valence electron. The values of $\langle r^2 \rangle$ were calculated in the Coulomb approximation [30].

Another model potential for the Rydberg–neutral interaction is the superposition of the polarization potential, $V_\mathrm{p} = -\alpha e^2/2R^4$, describing interaction of the perturber with the core of the Rydberg atom and the Fermi pseudopotential, $V_\mathrm{F} = 2\pi \left(\hbar^2/m\right) L\delta(\mathbf{r} - \mathbf{R})$, representing interaction between the perturber and the Rydberg electron (with $\mathbf{R}$ and $\mathbf{r}$ being the coordinates of the perturber and of the Rydberg electron, respectively, m the mass of the electron and L the electron-perturber scattering length). The broadening and shift cross sections taking into account only the isotropic part of the Fermi potential have been calculated as [11]

$$\sigma_\mathrm{b} = \begin{cases} 4\pi a_0^2 n^{*4}, & n^* < n_1^* = \left(|L|/4\tau_0 v\right)^{1/4} \\ 8\pi a_0^2 \frac{n_1^{*8}}{n^{*4}} \left(1 - \frac{n_1^{*8}}{2n^{*8}}\right), & n_1^* < n^* < 0.70 n_2^* \\ \sigma_{\mathrm{b,c}} + 8\pi a_0^2 \frac{n_1^{*8}}{n^{*4}} \left(1 - \left(\frac{\sigma_{\mathrm{b,c}}}{\pi a_0^2}\right)^{1/2} \frac{1}{2n^{*2}}\right), & \\ & n^* > 0.70 n_2^* \end{cases} \tag{11}$$

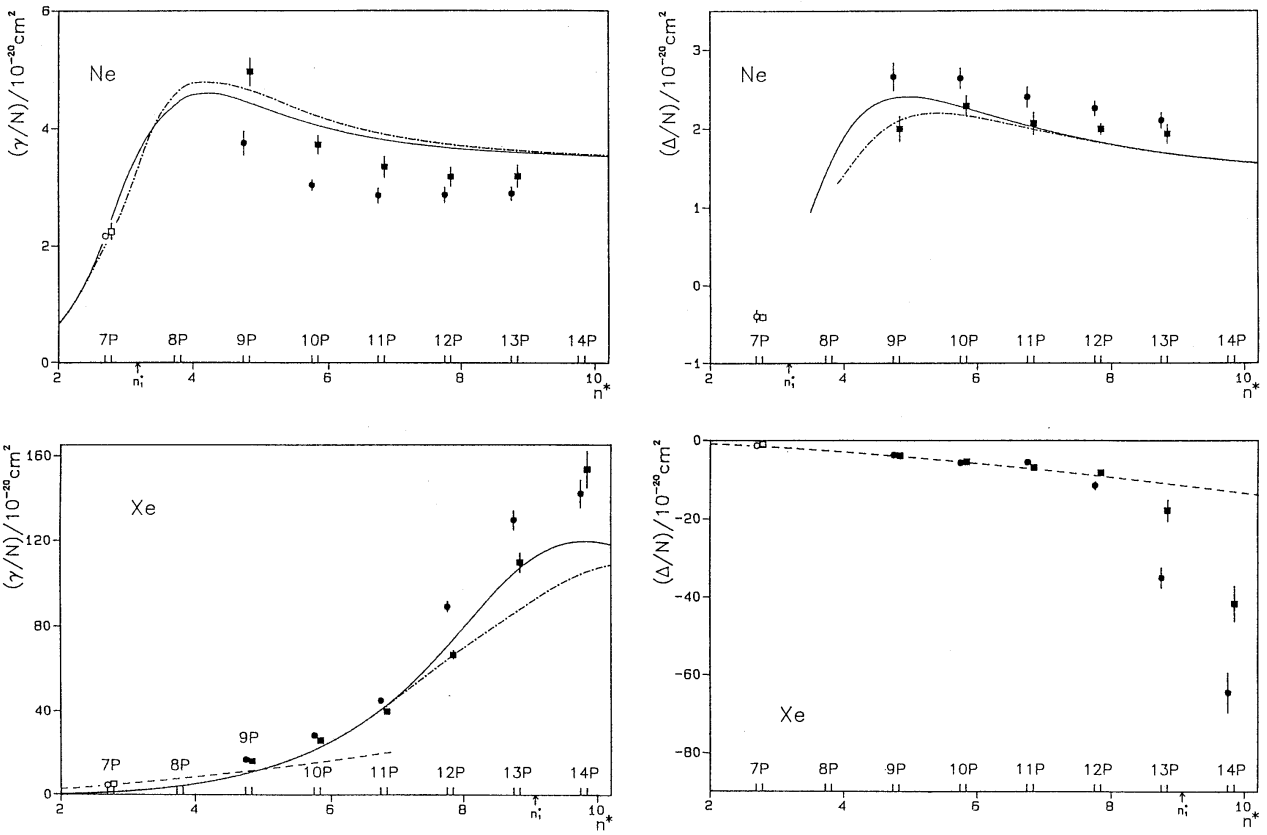

Fig. 3. Experimental broadening rates γ/N and shift rates Δ/N for the transitions Tl $6P_{1/2}$–$nP_{1/2}$ (•, ○) and Tl $6P_{1/2}$–$nP_{3/2}$ (■, □) ($n = 7$ [16]; 9 – 14) perturbed by Neon (Ne) and Xenon (Xe). Calculated rates for a Van der Waals potential (− − − −) and a superposition of a polarization and a Fermi potential ($P_{1/2}$: ————, $P_{3/2}$: − · − · −).

$$\sigma_{\rm s} = \begin{cases} \sim 0, & n^* < 1.09 n_1^* \\ \frac{2\pi\hbar L}{mv}\left(1-\frac{n_1^{*8}}{n^{*8}}\right) + \sigma_{\rm s,c}\left(\frac{v_0\alpha}{2a_0^3 v}\right)^{1/3}\left(\frac{n^{*6}}{2n_1^{*8}} - \frac{1}{n_1^{*2}}\right), & \\ & 1.09 n_1^* < n^* < 0.73 n_2^* \\ \frac{2\pi\hbar L}{mv}\left(1-\frac{n_1^{*8}}{n^{*8}}\right) + \sigma_{\rm s,c}\left[1-\left(\frac{v_0\alpha}{2a_0^3 v}\right)^{1/3}\frac{1}{n^{*2}}\right], & \\ & n^* > 0.73 n_2^*. \end{cases} \tag{12}$$

Here

$$\sigma_{\rm b,c} = 5.7\left(\frac{e^2\alpha}{2\hbar v}\right)^{2/3}, \quad \sigma_{\rm s,c} = -\sqrt{3}\sigma_{\rm b,c} \tag{13}$$

are the broadening and shift cross sections due to the polarization interaction between the perturber and the core of the Rydberg atom,

$$n_2^* = \left[\frac{|L|}{\left(a_0^3\alpha\right)^{1/6}\left(v/v_0\right)^{5/6}}\right]^{1/3},$$

while $a_0 = \hbar^2/me^2$, $\tau_0 = \hbar^3/me^4$ and $v_0 = e^2/\hbar$ are the atomic units of length (Bohr radius), time and velocity, respectively.

This theory in general and equations (11) and (12) in particular are widely used for analysis of experimental results and have been modified in different ways ([2, 3, 12-16, 21-23, 26, 33-37] and references given there).

According to this theory the broadening cross section $\sigma_{\rm b}$ as a function of the effective principle quantum number n^* of the upper state is proportional to n^{*4} for small n^*, reaches its maximum value $\sigma_{\rm b}^{\max} = \frac{16}{3}\sqrt{\frac{2}{3}}\pi a_0^2 n_1^{*4}$ at $n^* = \left(\frac{3}{2}\right)^{1/8} n_1^*$ and then decreases asymptotically for high n^* approaching the value $\sigma_{\rm b,c}$ owing to the pure core-perturber interaction. The shift cross section $\sigma_{\rm s}$ according to this theory is very small for $n^* \leq n_1^*$, then increases very rapidly with the increase of n^* in the region of $n^* \simeq n_1^*$, and reaches fast its asymptotic value $\sigma_{\rm s} = \sigma_{\rm s,e} + \sigma_{\rm s,c}$ (with $\sigma_{\rm s,e} = 2\pi\hbar L/mv$ being the shift cross section due to the Fermi interaction between the perturber and Rydberg electron) [11].

For comparison of the theory with experimental data we need the broadening and shift rates, γ/N and Δ/N, *i.e.* the cross sections averaged over the Maxwellian distribution of the relative velocity of the colliding atoms. For the broadening cross section the averaging was performed in paper [11]. For the shift cross section this has been done by Thompson *et al.* [15]. The averaging smooths a little bit the sharp dependences of the cross sections on the

principle quantum number in the region of $n^* \simeq n_1^*$. Thus, the broadening rate reaches a maximum at $n^* \simeq 1.08 n_1^*$ and this maximum is about 20% lower than the maximal value of $\sigma_\mathrm{b}(\bar{v})\,\bar{v}$, of the rate without averaging.

These results of papers [11] and [15] were used in this work for calculations of the broadening and shift rates of the $6\mathrm{P}_{1/2}$–$n\mathrm{P}_{1/2}$ lines. Values for the perturber scattering length L and the polarizability α applied in these calculations are given in Table 4.

The theoretical rates for the two considered potentials are presented in Table 1 together with the experimental results. Results for Ne and Xe perturbers are also plotted in Figure 3. Experimental results of Borstel *et al.* [16] for the $6\mathrm{P}_{1/2}$–$7\mathrm{P}_{1/2}$ line are added in this figure, too. Curves for He, Ar and Kr perturbers have already been presented [26].

The comparison of the experimental and theoretical data shows, that for Ar, Kr, and Xe perturbers the Van der Waals potential provides rates in agreement with the experimental data for transitions into states with small principle quantum numbers n. This is obvious for $n = 7$. With increasing n the experimental broadening rates become significantly larger those predicted by the Van der Waals potential for transitions into the 9P and higher levels. For shift rates, on the contrary, the agreement of the experimental values with predictions of the Van der Waals potential is extended to higher principle quantum numbers as it can be seen clearly for Kr perturbers up to $n = 10$ and for Xe up to $n = 11$.

This remarkable difference between line broadening and line shift is a result of the different regions of the impact parameter b, which provide the main contributions to γ/N or Δ/N. The line shift is mainly produced by collisions with relatively large impact parameters, where the interaction potential is well approximated by the long-range polarization potential even for spatially more extended states with higher n^*. This is especially true for Kr and Xe perturbers with large polarizabilities. For the line broadening, on the contrary, collisions with smaller b are most important and even for the 9P state the scattering interaction potential of the Tl valence electron with the rare gas atom penetrating into the electron shell must be taken into account.

Due to the small polarizability of He and Ne, the scattering of the valence electron by the perturbers is more important for the line shift and broadening by these gases even for small n. In combination with the positive scattering length, this results in the observed blue shift of the lines whereas red shifts are predicted by the Van der Waals potential.

Using the superposition of polarization and Fermi potentials in paper [11] the electron scattering by the perturbers has been taken into account. The theoretical rates obtained from the formulas (11) and (12) show the correct behaviour with increasing effective principle quantum number n^*. The maximum of the calculated broadening rates at $n^* = 1.08\,n_1^*$ is in agreement with the measured values. Very good agreement between the experimental and theoretical data is found for He, Ar, and Kr at $n^* > n_1^*$. For $n^* < n_1^*$ the superposition of the polarization and the Fermi potentials provides broadening rates in better agreement with the experiment than the Van der Waals potential if the extension of the wave function $2n^{*2}a_0$ exceeds the Weisskopf radius for the Van der Waals potential. The strong increase at $n^* \approx n_1^*$ and the asymptotic behaviour for larger n^* of the shift rates are correctly described by the theory [11], too.

However, some discrepancy between experimental and theoretical predictions of the shift by Xe at $n^* \simeq n_1^*$ is observed. Theoretical underestimation of the shift rates in such a case is due to some approximations in the theoretical analysis. The squared radial JWKB-wavefunctions used in [11], averaged over oscillations, are rough approximations for the states with small n^* and result in a jump of the phase shift $\eta_\mathrm{f}(b)$ at the classical radius of the Rydberg atom $b \simeq r_2 \simeq 2a_0 n^{*2}$ if $n^* \leq n_1^*$. Thereby, the deviations for small n^* may be explained. This results in the underestimation of the shift cross sections for $n^* \leq n_1^*$. An attempt to overcome this discontinuity of η_f taking into account the finite size of the perturber has been undertaken in [12].

Here we want to pay attention to another approach considered in [11] where the Fermi pseudopotential with the electron charge density uniformly spread out inside a sphere of radius r_2 has been introduced. The broadening and shift cross sections for such square-well potential may be expressed as

$$\sigma_\mathrm{b,sw} \simeq \begin{cases} 4\pi a_0^2 n^{*4}, & n^* \leq n_1^* \\ 9\pi a_0^2 \frac{n_1^{*8}}{n^{*4}} \left(1 - \frac{n_1^{*8}}{2n^{*8}}\right), & n^* > n_1^*, \end{cases} \tag{14}$$

$$\sigma_\mathrm{s,sw} \simeq \begin{cases} 0, & n^* \leq n_1^* \\ \frac{2\pi\hbar L}{mv} \left(1 - \frac{9}{10}\frac{n_1^{*8}}{n^{*8}}\right), & n^* > n_1^*. \end{cases} \tag{15}$$

We see that these cross sections are very similar to those given by equations (11) and (12) except of the shift cross section at $n^* \simeq n_1^*$. Therefore, this model yields the broadening and shift rates close to those given in Table 1 and Figure 3 except the shift rates by heavy rare gases at $n^* \simeq n_1^*$.

The averaging of the shift cross section (15) over the Maxwellian velocity distribution gives the shift rate

$$\frac{\Delta_\mathrm{sw}}{N} = \frac{2\pi\hbar L}{m}\left[\frac{2}{\sqrt{\pi}}\mathrm{e}^{-y}\sqrt{y} + (1 - 1.8y)\,\mathrm{erfc}\sqrt{y}\right] \tag{16}$$

where $y = L^2/4\pi\tau_0^2\bar{v}^2 n^{*8}$.

According to equation (16) the shift rates of the 13P and 14P states perturbed by Xe are -17×10^{-20} cm^2 and -53×10^{-20} cm^2, respectively, which are considerably closer to the experimental results than calculations with the Van der Waals potential and JWKB approximation.

Therefore, there is no essential disagreement between the experimental data and results of theoretical analysis in the whole range of quantum numbers and rare gases under consideration.

4.2 Dependence on the angular momentum

The measured broadening and shift rates of the Tl $6P_{1/2}$–$nP_{1/2,\ 3/2}$ lines show a significant dependence on the angular momentum J_f of the upper state indicating that the anisotropy of the interaction potential must be taken into account in the case of the $P_{3/2}$ states. Relative differences of the rates of up to 50% are observed between transitions into $nP_{1/2}$ and $nP_{3/2}$ states with the same principle quantum number n.

A theoretical analysis of the collisional broadening and shift of lines corresponding to transitions into upper levels with angular momentum $J_f \geq 1$ taking into account the anisotropy of the interaction potential is given in paper [13]. For the superposition of a polarization and a Fermi pseudopotential the diagonal elements of the collision S matrix have been approximately calculated. After that the broadening and shift cross sections depending on the angular momentum J_f were derived according to equations (4) and (5). These cross sections are related with the cross sections $\sigma_{b,s}(\alpha, L)$ given by equations (11) and (12) for the isotropic part of the considered potential. For $P_{1/2}$ and $P_{3/2}$ states we have [13]

$$\sigma_{b,s}(P_{1/2}) = \sigma_{b,s}(\alpha, L) \tag{17}$$

$$\sigma_{b,s}(P_{3/2}) = 1/2\left[\sigma_{b,s}(\alpha, L/2) + \sigma_{b,s}(\alpha, 3L/2)\right]. \tag{18}$$

Equations (17) and (18) are valid for both broadening and shift cross sections.

The results of this theory may be explained as follows. While in case of isotropic $nP_{1/2}$ states each collision with a given collision parameter b produces the same phase shift, in case of $nP_{3/2}$ states collisional trajectories near the nodal surfaces of the anisotropic wave function result in smaller phase shifts and others in larger ones than for $nP_{1/2}$. For $n^* < n_1^*$ the contributions of collisions with smaller phase shifts result in the deviations for the $nP_{3/2}$ broadening rates compared to the isotropic $nP_{1/2}$ states. Collisions with larger phase shifts that totally destroy the optical coherence, even for $n^* > n_1^*$, cause the shift of the maximum of the $nP_{3/2}$ broadening rates towards higher n^*.

The largest differences of the shift rates may be observed at effective principle quantum numbers near n_1^*. For $nP_{1/2}$ states with such principle quantum numbers all collision geometries with collision parameters b in a certain range near $2{n^*}^2 a_0$ result in phase shifts $\eta < \pi$ that are significant for contributing to line shift. The smaller $nP_{3/2}$ shift rates result from collisions with small phase shifts, which only yield very small line shift contributions, or from collisions with large phase shifts $\eta > \pi$. Such collisions destroy the optical coherence but do not contribute to line shift.

The resulting rates for the $6P_{1/2}$–$nP_{3/2}$ lines are presented in Table 1 and Figure 3, too. The differences in the calculated broadening and shift rates between the $6P_{1/2}$–$nP_{1/2}$ and the $6P_{1/2}$–$nP_{3/2}$ lines agree with the experimental data. The broadening rates coincide within the limits of error for very small principle quantum numbers, but with increasing n^* they are smaller for $6P_{1/2}$–$nP_{3/2}$ than for $6P_{1/2}$–$nP_{1/2}$ lines. In the vicinity of n_1^* this ratio of the observed broadening rates inverts and with further increase of n^* γ/N is larger for transitions to $nP_{3/2}$ states than for transitions to $nP_{1/2}$ states. This characteristic dependence on n^* can be best seen for the Kr perturbers.

As predicted by the theory the absolute value of the experimental shift rates is smaller for the $6P_{1/2}$–$nP_{3/2}$ lines than for the $6P_{1/2}$–$nP_{1/2}$ lines with the same n or agree within the limits of error. Large differences are observed at effective principle quantum numbers in the vicinity of n_1^* except for Ar perturbers.

It is instructive to consider in more detail the line shifts by Ar, Kr, or Xe. For small n^* the differences between the shift rates for $nP_{1/2}$ and $nP_{3/2}$ states are small as long as the rates can properly be calculated by means of the Van der Waals potential. This is in accord with the results of an estimation done for an anisotropic Van der Waals potential of the form [38,39] $V(\mathbf{R}, \mathbf{r}) = -\alpha e^2 r^2 R^{-6}(P_0 + P_2)$ (where $P_k(\mathbf{R}, \mathbf{r}/Rr)$ are the Legendre functions) and providing differences of the shift rates of less than 1%. Considerable discrepancies between the shift rates of $6P_{1/2}$–$nP_{1/2}$ and $6P_{1/2}$–$nP_{3/2}$ lines are observed with increasing n^* just for those principle quantum numbers for which the experimental rates deviate from the predictions for the Van der Waals potential. As the deviations are caused of the valence electron scattering by the perturber, this interaction must be considered as the principle reason for the angular momentum dependence of the line shifts, too. This statement is in agreement with the theoretical analysis in [13].

4.3 Dependence on the rank of the transition operator

A theoretical analysis of pressure broadening including the dependence on the rank of the transition operator is given by Cooper [17] and in more detail using a density matrix formulation by Omont [18,19]. They found two necessary conditions for the observation of rank dependent broadening and shift rates. The angular momenta $J_{i,f}$ of the initial and the final state of the transition must be equal or more than one, $J_{i,f} \geq 1$, implying anisotropic interaction potentials for both states involved in the transition and the perturbation of both states must significantly contribute to the line broadening and shift. Furthermore, Omont predicted that under these conditions the lines of a hyperfine multiplet should have different broadening and shift rates.

Our measurements on the $6P_{3/2}$–$9P_{3/2}$ transition done for quadrupolar as well as for mainly scalar excitation show no significant rank dependence of the rates (see Tab. 3). For both kinds of excitation the broadening and shift rates of all considered hyperfine structure lines agree within the limits of error contrary to a guess made in paper [16]. We performed these measurements with He and Ar perturbers in order to investigate a repulsive as well as an attractive collisional system.

Whereas the condition $J_{i,f} \geq 1$ is satisfied in the case of the $6P_{3/2}$–$9P_{3/2}$ transition, it must be assumed that due to the larger extension of the $9P_{3/2}$ state wavefunction compared to that of the $6P_{3/2}$ state, the

perturbation of the lower state can be neglected in pressure broadening considerations and, therefore, the rank dependence vanishes. This is a usual assumption in the literature for transitions between the ground state and higher excited states. The negligible contribution of the $6P_{3/2}$ state can further be proved by comparing the transitions $6P_{1/2}$–$9P_{3/2}$ and $6P_{3/2}$–$9P_{3/2}$. The broadening and shift rates of these transitions coincide within the limits of error.

These results also justify the neglect of the interaction between the perturbers and Tl atoms in the lower state in the discussion of the broadening and shift of the $6P_{1/2}$–$nP_{1/2,\ 3/2}$ lines in Sections 4.1 and 4.2.

5 Conclusions

Although we have found quite good qualitative agreement between the experimental data and the results of the calculations the quantitative comparison shows some typical perturber independent deviations indicating that the theory can be further improved:

- The maximum of the calculated broadening rates is larger for transitions into isotropic $nP_{1/2}$ states than for transitions into anisotropic $nP_{3/2}$ states, but it is vice versa for the measured rates. A similar behaviour of the experimental data was found for n'S–nS and n'S–nD lines of alkali-metals broadened by rare gases [14,40], too.
- Near $n^* = n_1^*$ the ratio of the broadening rates for the $6P_{1/2}$–$nP_{1/2}$ and the $6P_{1/2}$–$nP_{3/2}$ lines inverts with the increase of the principle quantum number n^*. This inversion is found for smaller principle quantum numbers than predicted by the theoretical analysis.
- The differences of the calculated rates between transitions into $nP_{1/2}$ and $nP_{3/2}$ states are smaller than the measured differences.

It should be noted, however, that it is the advantage of the approximate solution given in [13] to provide analytical expressions for the broadening and shift rates explicitly showing their dependence on the effective principle quantum number.

Further improvement of the theoretical analysis may be achieved by a more sophisticated calculation of the relevant collision S matrix elements.

The observed independence of the broadening and shift rates of the transition Tl $6P_{3/2}$–$9P_{3/2}$ on the rank of transition operator justifies the neglect of the interaction between the perturbers and the radiator in the lower state in the calculations of the line broadening and shift for transitions from the ground state even to low Rydberg states.

References

1. S.Y. Ch'en, M. Takeo, Rev. Mod. Phys. **29**, 20 (1957).
2. B. Kaulakys, P. Serapinas, Lit. Fiz. Sb. **24**(3), 3 (1984); Sov. Phys. -Collec. (Allerton Press, Inc.) **24**(3), 1 (1984).
3. I.L. Beigman, V.S. Lebedev, Phys. Rep. **250**, 95 (1995).
4. E.L. Lewis, Phys. Reports **58**, 1 (1980).
5. N. Allard, J. Kielkopf, Rev. Mod. Phys. **54**, 1103 (1982).
6. I.I. Sobelman, L.A. Vainshtein, E.A. Yukov, Excitation of Atoms and Broadening of Spectral Lines (Berlin, Heidelberg, New York, Springer 1981).
7. E. Fermi, Nuovo Cimento **11**, 157 (1934).
8. O.B. Firsov, ZhETF **21**, 627, 634 (1951).
9. V.V. Alekseev, I.I. Sobelman, ZhETF **49**, 1274 (1965); Sov. Phys. -JETP **22**, 882 (1966).
10. A. Omont, J. Phys. France **38**, 1343 (1977).
11. B. Kaulakys, J. Phys. B **17**, 4485 (1984).
12. G. Hermann, Phys. Lett. A **133**, 225 (1988).
13. G. Hermann, B. Kaulakys, G. Lasnitschka, G. Mahr, A. Scharmann, J. Phys. B **25**, L407 (1992).
14. R. Kachru, T.W. Mossberg, S.R. Hartmann, Phys. Rev. A **21**, 1124 (1980).
15. D.C. Thompson, E. Kammermayer, B.P. Stoicheff, E. Weinberger, Phys. Rev. A **36**, 2134 (1987).
16. M.V. Borstel, G. Hermann, G. Lasnitschka, Z. Phys. D **9**, 15 (1988).
17. J. Cooper, Rev. Mod. Phys. **39**, 167 (1967).
18. A. Omont, J. Phys. France **34**, 179 (1973).
19. A. Omont, Prog. Quantum Electronics **5**, 69 (1977).
20. B. Cheron, R. Scheps, A. Gallagher, Phys. Rev. A **15**, 651 (1977).
21. E. Lisicki, A. Bielski, J. Szudy, J. Wolnikowski, Z. Naturforsch. **40a**, 800 (1985).
22. R.S. Dygdala, R. Bobkowski, E. Lisicki, J. Phys. B **22**, 1563 (1989) and references given there.
23. R.S. Dygdala, E. Lisicki, Phys. Scr. **37**, 38 (1988).
24. K. Naveedullah, Nuovo Cim. D **11**, 1349 (1989) and references given there.
25. K. Naveedullah, Nuovo Cim. D **9**, 1463 (1987).
26. G. Mahr, G. Hermann, Phys. Rev. A **54**, 2775 (1996).
27. G. Grynberg, F. Biraben, E. Giacobino, B. Cagnac, J. Phys. France **38**, 629 (1977).
28. W.R. Hindmarsh, J.M. Farr, Prog. Quantum Electronics **2**, 141 (1972).
29. G. Peach, Adv. Phys. **30**, 367 (1981); J. Phys. B **17**, 2599 (1984).
30. H.A. Bethe, E.E. Salpeter, Quantum Mechanics of One- and Two-Electron-Atoms (Heidelberg, Springer 1957).
31. R.R. Teachout, R.T. Pack, At. Data **3**, 195 (1971).
32. K.S. Golovanivskiĭ, A.P. Kabilan, Sov. Phys. JETP **53**, 1153 (1981).
33. R.S. Trawinski, A. Bielski, A., J. Phys. B **26**, 4789 (1993).
34. R.S. Trawinski, A. Bielski, J. Szudy, J. Wolnikowski, Acta Phys. Pol. A **86**, 333 (1994).
35. H. Van Regemorter, J. Phys. B **27**, 3863 (1994).
36. D. Hoang-Binh, H. Van Regemorter, J. Phys. B **28**, 3147 (1995).
37. P.J. Leo, D.F.T. Mullamphy, G. Peach, V. Ventur, I.B. Whittingham, J. Phys. B **30**, 535 (1997).
38. W.E. Baylis, J. Chem. Phys. **51**, 2665 (1969).
39. G.D. Mahan, J. Chem. Phys. **50**, 2755 (1969).
40. K.H. Weber, K. Niemax, Z. Phys. A **307**, 13 (1982).